


## Instanton induced transverse single spin asymmetry for $\pi^0$ production in $pp$ scattering

Nikolai Korchagin<sup>1,\*</sup>, Nikolai Kochelev,<sup>‡</sup> and Pengming Zhang<sup>2,†</sup>

<sup>1</sup>*Institute of Modern Physics, Chinese Academy of Sciences, Lanzhou 730000, China*

<sup>2</sup>*School of Physics and Astronomy, Sun Yat-sen University, Zhuhai 519082, China*

 (Received 25 December 2020; accepted 11 January 2021; published 15 February 2021)

We calculate the production cross section and the transverse single-spin asymmetry for pion in  $p^\uparrow + p \rightarrow \pi^0 + X$ . Our computation is based on existence of the instanton induced effective quark-gluon and quark-gluon-pion interactions with a strong spin dependency. In this framework we calculate the cross section without using fragmentation functions. We compare predictions of the model with data from RHIC. Our numerical results, based on the instanton liquid model for QCD vacuum, are in agreement with unpolarized cross section data. The asymmetry grows with the transverse momentum of pion  $k_t$  in accordance with experimental observations. It reaches a value  $\sim 10\%$  but at higher  $k_t$  than experiment shows.

DOI: [10.1103/PhysRevD.103.034012](https://doi.org/10.1103/PhysRevD.103.034012)

### I. INTRODUCTION

Transverse single-spin asymmetries (TSSAs) have been puzzling physicists more than three decades. They are among the most intriguing observables in hadronic physics since first FermiLab measurements for  $p + \text{Be} \rightarrow \Lambda^\uparrow + X$  reaction [1]. Since then, TSSA are observed in many different reactions, including mesons production in  $pp$  and SIDIS. Results of experiments are in contradiction with predictions from the perturbative quantum chromodynamics (pQCD) and the naive collinear parton model. It was expected that asymmetries should be extremely small [2]. For comprehensive introduction to the problematic we refer the reader to review [3]. In this paper we focus on transverse single-spin asymmetry for pion production in nucleon-nucleon scattering. It is often called analyzing power and denoted as  $A_N$ . Such measurements were done at FermiLab by E581/E704 Collaborations [4]. Later, similar measurements at higher energy was performed at RHIC [5]. Unambiguous effects were measured and they triggered renewed interest on TSSAs.

A popular approach to describe observed spin effects is based on the extension of the collinear parton model with inclusion of parton's transverse motion. It utilizes the transverse momentum dependent (TMD) factorization

scheme. However, the factorization theorem has not been proven generally for such case [6]. It has so far only been proven for some classes of processes: the Drell-Yan ( $q + \bar{q} \rightarrow l^+ + l^-$ ) [7] and semi-inclusive DIS [8].  $k_T$ -dependent factorization is, therefore, an assumption, although a well-accepted one. Efforts are ongoing to establish the theoretical basis more firmly. We refer the reader to papers with discussions of the universality [9–12] and TMD pdf's evolution [13,14]. Moreover, the dominance of  $k_T$  effects among other contributions is disputed. For example, effects of parton virtuality, target mass corrections could be of the same order of magnitude as transverse parton motion [15].

Two mechanisms for TSSA have been proposed in the framework of noncollinear parton model. The first is the Collins mechanism, when transversity distribution in combination with spin-dependent, chiral-odd fragmentation function (FF) can give rise TSSA [16]. The Collins FF describes the azimuthal asymmetry of a fragmented hadron in respect to struck quark polarization. Work [17,18] has suggested that it is difficult to explain the large TSSA entirely in terms of the Collins effect.

The second mechanism was suggested by Sivers [19]. The idea is that parton distributions are asymmetric in the intrinsic transverse momentum  $k_T$  within the proton. The Sivers effect can exist both for quarks and gluons. This intrinsic asymmetry is represented by the Sivers function of the unpolarized partons in a transversely polarized proton. Calculations based on the Sivers effect for E704 data and other results can be found in [20,21].

Other direction for investigation is the twist-3 approach. It was pointed out that three-parton correlators may give rise to TSSAs [22]. Qiu and Sterman examined higher-twist

\*korchagin@impcas.ac.cn

†zhangpm5@mail.sysu.edu.cn

‡Deceased.

*Published by the American Physical Society under the terms of the Creative Commons Attribution 4.0 International license. Further distribution of this work must maintain attribution to the author(s) and the published article's title, journal citation, and DOI. Funded by SCOAP<sup>3</sup>.*

contributions due interference between quark and gluon fields in the initial polarized proton [23]. Similar study was performed by Kanazawa and Koike for quark-gluon interference in the final state[24].

In the present paper we propose an alternative mechanism for TSSA in  $pp \rightarrow \pi X$ , based on the existence of novel effective interaction induced by instantons. The instantons describe sub-barrier transitions between the classical QCD vacua with different topological charges. In previous work [25] we calculated TSSA for quark-quark scattering and showed that such mechanism gives significant TSSA. However, generalization of that result to the case of real hadron scattering is unclear. Calculation in the standard, pQCD-like way with introduction of fragmentation functions is not self-consistent. Extraction of FFs requires an evolution equation and was done in the framework of pQCD without considering an additional nonperturbative low-energy interaction. The new vertex may give significant contribution to the evolution [26]. Reanalyzing data with the new vertex and modified evolution will not give new information since we will introduce more parameters.

Fortunately, the low-energy effective interaction generated by instantons provides us the other solution. It contains a pion-quark-gluon vertex. In such case, we do not need any fragmentation function and, as a result, we reduce the number of parameters in the model. Formation of pion happens at the short distance of the instanton scale  $\approx 0.3$  fm, which is smaller than distances of confinement dynamics. The other important consequence is breaking of the pQCD factorization. Scattering of partons and hadronization are coherent at the instanton scale. It might be a cornerstone of various phenomena observed in high energy reactions in the few GeV range for the transferred momentum.

This paper has the following structure. Section II gives a brief introduction to the instanton generated interaction. In Sec. III we discuss calculation for pion production cross-section and then, in Sec. IV, we calculate TSSA. Section V is dedicated to numerical analysis and discussion.

## II. INSTANTON GENERATED INTERACTION

Our calculation for TSSA is based on the presence of the intrinsic spin-flip during the quark-gluon interaction already on the quark level. The generating functional for such nonperturbative interaction was obtained previously [27]. Later it was generalized in order to preserve the chiral invariance [28]. The generalized interaction Lagrangian has the form

$$\mathcal{L}_I = -ig_s \frac{\mu_a}{4m_q} \bar{\psi} t^a [\sigma_{\mu\nu} e^{i\gamma_5 \vec{\tau} \vec{\phi}/F_\pi}] \psi G_{\mu\nu}^a, \quad (1)$$

where  $g_s$  is the strong coupling constant,  $\mu_a$  is the anomalous quark chromomagnetic moment(AQCM),  $m_q$  is the constituent quark mass,  $t^a$  are  $SU(3)$  color matrices,

$\sigma_{\mu\nu} = \frac{1}{2}[\gamma_\mu, \gamma_\nu]$ ,  $\vec{\tau}$  are Pauli matrices acting in the flavor space,  $\vec{\phi}$  is the pion field,  $F_\pi = 93$  MeV is the pion decay constant.  $G_{\mu\nu}^a$  is the gluon field strength. This effective interaction is obtained by expanding t' Hooft interaction in the power series in the gluon field strength, assuming a big spatial size of the gluon fluctuations.

Based on the Lagrangian (1), the full interaction vertex is

$$U_\mu^a = ig_s t^a (\gamma_\mu - \sigma_{\mu\nu} q_\nu F(k_1, k_2, q) e^{i\gamma_5 \vec{\tau} \vec{\phi}/F_\pi}). \quad (2)$$

The first term  $\gamma_\mu$  corresponds to usual pQCD interaction. The second term is from effective low-energy action Eq. (1).  $k_{1,2}$  are the momenta of incoming and outgoing quarks,  $q = k_2 - k_1$ . The form factor  $F$  is calculated in the instanton liquid model [28,29]:

$$\begin{aligned} F(k_1, k_2, q) &= \frac{\mu_a}{2m_q} \Phi_q \left( \frac{|k_1| \rho_c}{2} \right) \Phi_q \left( \frac{|k_2| \rho_c}{2} \right) F_g(|q| \rho_c), \\ \Phi_q(z) &= -z \frac{d}{dz} (I_0(z) K_0(z) - I_1(z) K_1(z)), \\ F_g(z) &= \frac{4}{z^2} - 2K_2(z), \end{aligned} \quad (3)$$

where are the  $I_\nu(z)$  and  $K_\nu(z)$  are the modified Bessel functions.  $\rho_c \approx 1.67$  GeV $^{-1}$  (1/3 fm) is the average instanton size. In our calculations all quarks are on mass shell, therefore  $\Phi_q = 1$  and we will omit it further.

The AQCM  $\mu_a$  is calculated in the framework of the instanton liquid model [27] is

$$\mu_a = -\frac{3\pi(m_q \rho_c)^2}{4\alpha_s(\rho_c)}. \quad (4)$$

AQCM in pQCD appears at higher order  $\alpha_s$  corrections. Therefore, it has a small value  $\mu_{\text{pQCD}} = \alpha_s/2\pi \approx 10^{-2}$ . In contrast, the instanton generated AQCM is of the order of 1. Moreover, instanton liquid model gives the sign of AQCM and, in its turn, determines the sign of observed TSSA. Equation (4) is obtained in the massless chiral limit. One should not be confused that the  $\mu_a$  increases with the quark mass.  $m_q$  is the constituent mass and this equation could not be applied for heavy  $c$ ,  $b$ , and  $t$  quarks.

If we expand the exponent in Eq. (2) into series and cut it on the second term, we get three types of vertices: traditional perturbative, chromomagnetic, and the vertex with pion,

$$\begin{aligned} U_\mu^a &= ig_s t^a \left( \gamma_\mu - \sigma_{\mu\nu} q_\nu F(k_1, k_2, q) \right. \\ &\quad \left. - i \frac{\vec{\tau} \vec{\phi}}{F_\pi} \gamma_5 \sigma_{\mu\nu} q_\nu F(k_1, k_2, q) \right). \end{aligned} \quad (5)$$

We neglect the higher order terms. Their contribution to the cross section is expected to be suppressed in the large  $N_c$

limit by factor  $1/N_c$  because  $F_\pi \sim \sqrt{N_c}$  [30]. Moreover, due to increasing of the final particles number, it should be suppressed at large  $x_F$  where TSSA is observed.

### III. CALCULATION OF CROSS SECTION

We are interested in process  $p^\uparrow p \rightarrow \pi X$ . Three parton subprocesses give contribution to the cross section. They are shown on Fig. 1. The diagram (a) was calculated before in [31] using an assumption that the pion fragments in the same kinematic region as the quark  $q_+$ , i.e., the pion and quark flight approximately in the same direction. In the present work we implement more rigorous calculation for the phase space and calculate additional contributions shown on panels (b) and (c) of Fig. 1. The contribution (b) has the chromomagnetic vertex on the bottom quark line instead of the perturbative one. The diagram (c)  $q + q \rightarrow 2\pi + 2q$  is essentially different. In our model we have the pion directly in the interaction vertex and should consider the process where the pion is inside of an unobserved inclusive state  $X$ . As the first step we study the partonic cross section and its features. Then we calculate the hadron cross section as convolution of partonic one with parton densities.

#### A. Parton cross section

In massless limit the parton cross section is

$$d\hat{\sigma} = \frac{|\mathcal{M}|^2}{2\hat{s}} d\hat{R}_i, \quad (6)$$

where  $d\hat{R}_i$  is the phase space for  $i$  number of particles. In our case it can be three  $d\hat{R}_3$  and four  $d\hat{R}_4$ . We use the hat symbol to emphasize that the phase space is expressed in terms of momenta and energies calculated in the *parton* c.m. frame. This frame moves in respect to the hadron c.m. frame.  $\hat{s}$  is the total energy of colliding partons.

In calculation we use the following Sudakov decomposition for momentum vectors:

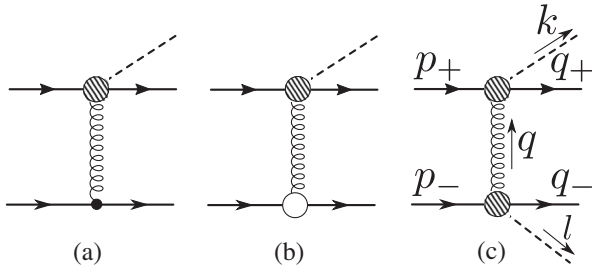


FIG. 1. Contributions to the pion production cross section and notation for momenta. The small dot denotes the perturbative vertex. The white blob is for the instanton induced interaction, it corresponds to the second term in Eq. (5). The shaded blob corresponds to the last term in Eq. (5) with the pion. Sub-figures correspond to scattering amplitudes  $\mathcal{M}_{(a,b,c)}$  respectively.

$$\begin{aligned} k &= xp_+ + \beta_k p_- + k_\perp, \\ q_+ &= \alpha_+ p_+ + \beta_+ p_- + q_{+\perp}, \\ q_- &= \alpha_- p_+ + \beta_- p_- + q_{-\perp}, \\ q &= \alpha p_+ + \beta p_- + q_\perp, \\ l &= \alpha_l p_+ + z p_- + l_\perp. \end{aligned} \quad (7)$$

$x$  and  $z$  are parts of longitudinal momentum of the initial quarks carried by  $k$  and  $l$  pions correspondingly.  $p_+$  and  $p_-$  are light-cone vectors:

$$\begin{aligned} p_+ &= (\sqrt{\hat{s}}/2, \sqrt{\hat{s}}/2, 0_\perp), & p_- &= (\sqrt{\hat{s}}/2, -\sqrt{\hat{s}}/2, 0_\perp), \\ \hat{s} &= (p_+ + p_-)^2, & p_+^2 &= p_-^2 = 0. \end{aligned} \quad (8)$$

Using this momenta decomposition the phase space  $d\hat{R}_3$  becomes

$$d\hat{R}_3 = \frac{1}{4(2\pi)^5} \frac{dx d^2 k_\perp d^2 q_\perp}{x(1-x)\hat{s}}. \quad (9)$$

Integration over the transverse transferred momenta  $q_\perp$  can be transformed to integration over the invariant mass  $M_k^2 = (k + q_+)^2$ :

$$d\hat{R}_3 = \frac{1}{2^7 \pi^5} \frac{dx d^2 k_\perp}{x^2 \hat{s}} \int_0^{E_{\text{sph}}^2} dM_k^2 \int_0^\pi d\tilde{\phi}, \quad (10)$$

where  $E_{\text{sph}}$  is the sphaleron energy,  $\tilde{\phi}$  is the azimuthal angle of an auxiliary vector  $\tilde{q}_\perp = xq_\perp - k_\perp$  (see Appendix A for details).

Sphaleron energy  $E_{\text{sph}} = \frac{3\pi}{2\rho_c}$  [28,32] determines the height of potential barriers between different topological vacuums. Instanton describes tunneling through that barrier, therefore the instanton induced vertex works only at energies less than the height of the barrier.

For diagram Fig. 1(c) we need the 4-particle phase space. Using Sudakov decomposition (7) it is

$$d\hat{R}_4 = \frac{dx dz d^2 k_\perp d^2 l_\perp d^2 q_\perp}{8(2\pi)^8 \hat{s} x(1-x)z(1-z)}. \quad (11)$$

Similar to  $d\hat{R}_3$ , we change integration over transverse momenta to integration over the invariant mass  $M_l^2 = (l + q_-)^2$ ,  $d^2 l_\perp \rightarrow dM_l^2 d\phi$ . Notice that here we replace  $d^2 l_\perp$ , not  $d^2 q_\perp$ ,

$$d\hat{R}_4 = \frac{dx dz d^2 k_\perp d^2 q_\perp dM_l^2}{2^{11} \pi^7 \hat{s} x(1-x)}. \quad (12)$$

Next step is calculation transition amplitudes  $\mathcal{M}_{(a,b,c)}$ . A letter corresponds to a panel on Fig. 1. The amplitude for the first diagram Fig. 1(a) is

$$|\mathcal{M}_{(a)}|^2 = \sum_{f,s,c} g_s \frac{C(q^2)}{F_\pi} (\bar{u}_{q_+} \sigma_{\mu\lambda} q_\lambda \gamma_5 t^a u_{p_+}) \times (\bar{u}_{q_-} i\gamma_\nu t^a u_{p_-}) D_{\mu\nu}^{aa'}(q^2) \times [\text{H.c.}], \quad (13)$$

where  $\sum_{f,s,c}$  short-notes averaging over spin, color, and flavor summation for corresponded pion ( $\pi^0$ ,  $\pi^\pm$ ).  $D_{\mu\nu}^{aa'}(q^2) = -ig_{\mu\nu}\delta^{aa'}/q^2$  is the gluon propagator.  $C(q^2)$  can be thought as an effective coupling:

$$C(q^2) = g_s \frac{\mu_a}{2m_q} F_g(q^2) = -\frac{3\pi^{3/2}\rho_c^2 m_q}{4\sqrt{\alpha_s(\rho_c)}} F_g(q^2). \quad (14)$$

Note that  $\alpha_s$  in the nonperturbative vertex is taken at the instanton size scale. This is the reason why we keep one  $g_s$  inside of  $C(q^2)$  and another, from perturbative vertex, outside. They supposed to be taken at different scales. Further, we will omit writing  $q$ -dependency of  $C$  for shortness.

We are interested in forward scattering. At such kinematics, for simplicity of calculation, we use Gribov's decomposition for  $g_{\mu\nu}$  in the gluon propagator.

$$g_{\mu\nu} = \frac{2p_{+\mu}p_{-\nu}}{\hat{s}} + \frac{2p_{+\nu}p_{-\mu}}{\hat{s}} + g_{\mu\nu}^\perp \approx \frac{2p_{+\mu}p_{-\nu}}{\hat{s}}. \quad (15)$$

Such decomposition allows us to isolate the leading contributions to an amplitude in the power of  $\hat{s}$  and factorize fermion traces. Using it we get for the amplitude (see Appendix B)

$$|\mathcal{M}_{(a)}|^2 = \sum_f \frac{8}{9} g_s^2 \frac{C^2 \hat{s}^2 (1-x)}{F_\pi^2 q_\perp^2}. \quad (16)$$

We keep the sum over flavor to indicate that expressions for  $\pi^\pm$ ,  $\pi^0$  are different.

In the case of the diagram Fig. 1(b), the difference is only in the trace over the bottom line,

$$|\mathcal{M}_{(b)}|^2 = \sum_{f,s,c} \frac{C^2}{F_\pi} (\bar{u}_{q_+} \sigma_{\mu\lambda} q_\lambda \gamma_5 t^a u_{p_+}) \times (\bar{u}_{q_-} i\sigma_{\nu\rho} q_\rho t^a u_{p_-}) D_{\mu\nu}^{aa'}(q) \times [\text{H.c.}] = \sum_f \frac{8C^4}{9F_\pi^2} \hat{s}^2 (1-x). \quad (17)$$

Notice that now the amplitude is proportional to  $C^2$ , not  $g_s C$ .

The amplitude for the two pion contribution  $q+q \rightarrow 2\pi+2q$  Fig. 1(c) is very similar to the case with one pion vertex. Now, the trace over the bottom fermion line is similar to the upper one.

$$|\mathcal{M}_{(c)}|^2 = \sum_{f,s,c} -\frac{C^2}{F_\pi^2} (\bar{u}_{q_+} \sigma_{\mu\lambda} q_\lambda \gamma_5 t^a u_{p_+}) \times (\bar{u}_{q_-} \sigma_{\nu\rho} q_\rho \gamma_5 t^a u_{p_-}) D_{\mu\nu}^{aa'} \times [\text{H.c.}] = \sum_f \frac{8C^4}{9F_\pi^4} \hat{s}^2 (1-x)(1-z). \quad (18)$$

Final formulas for contributions to the parton cross section shown on Fig. 1 are

$$d\hat{\sigma}_{(a)} = \sum_f \int_0^{E_{\text{sph}}^2} dM_k^2 \int_0^\pi d\tilde{\phi} \frac{g_s^2 C^2}{9(2\pi)^5 F_\pi^2} \frac{1-x}{q_\perp^2 x^2} dx d^2 k_\perp, \quad (19)$$

$$d\hat{\sigma}_{(b)} = \sum_f \int_0^{E_{\text{sph}}^2} dM_k^2 \int_0^\pi d\tilde{\phi} \frac{C^4}{9(2\pi)^5 F_\pi^2} \frac{1-x}{x^2} dx d^2 k_\perp, \quad (20)$$

$$d\hat{\sigma}_{(c)} = \sum_f \int_0^{E_{\text{sph}}^2} dM_k^2 \int_0^\pi d\tilde{\phi} \frac{C^4 E_{\text{sph}}^2}{92^{10} \pi^7 F_\pi^4} \frac{(1-x)}{x^2} dx d^2 k_\perp. \quad (21)$$

The detailed derivation of this equation is given in Appendix B.

## B. $pp \rightarrow \pi X$ cross section

The next step is to calculate observables on the hadron level. Differential hadron cross section is a convolution of parton distribution functions (PDF) and the parton cross section

$$E_k \frac{d\sigma}{d^3 k} = \sum_f \int_{x_a^{\min}}^{x_a^{\max}} dx_a \int_{x_b^{\min}}^{x_b^{\max}} dx_b f(x_a) f(x_b) \frac{2E_k}{\sqrt{s} x_a} \frac{d\hat{\sigma}}{dx d^2 k_\perp}. \quad (22)$$

The flavor sum  $\sum_f$  indicates the proper summation for a corresponding pion. The explicit formula for the  $\pi^0$  production cross section is

$$E_k \frac{d\sigma}{d^3 k} = 3 \iint dx_a dx_b (f_u(x_a) + f_d(x_a)) \times (f_u(x_b) + f_d(x_b)) \frac{\sqrt{x_T^2 + x_F^2}}{x_a} \frac{d\hat{\sigma}_{(c)}}{dx d^2 k_\perp} + \iint dx_a dx_b (f_u(x_a) + f_d(x_a)) \times (f_u(x_b) + f_d(x_b)) \frac{\sqrt{x_T^2 + x_F^2}}{x_a} \frac{(d\hat{\sigma}_{(a)} + d\hat{\sigma}_{(b)})}{dx d^2 k_\perp}. \quad (23)$$

Factor 3 in the first line is the result of summation over unobserved pions ( $\pi^\pm, \pi^0$ ) in inclusive state  $X$ , produced from the bottom vertex Fig. 1(c). In the case of  $\pi^+$  production the cross section is

$$E_k \frac{d\sigma}{d^3k} = 6 \iint dx_a dx_b f_u(x_a) (f_u(x_b) + f_d(x_b)) \times \frac{\sqrt{x_T^2 + x_F^2}}{x_a} \frac{d\hat{\sigma}_{(c)}}{dx d^2k_\perp} + 2 \iint dx_a dx_b f_u(x_a) (f_u(x_b) + f_d(x_b)) \times \frac{\sqrt{x_T^2 + x_F^2}}{x_a} \frac{(d\hat{\sigma}_{(a)} + d\hat{\sigma}_{(b)})}{dx d^2k_\perp}. \quad (24)$$

$\pi^-$  cross section is given by replacing  $f_u(x_a) \rightarrow f_d(x_a)$ .

In order to determine integration limits for  $x_{a,b}$ , notice that one could reduce  $2 \rightarrow 3$  and  $2 \rightarrow 4$  parton subprocesses to the  $2 \rightarrow 2$  case if combines all particles except the detected pion into an effective particle with the mass square  $X^2$ . We could not neglect this invariant mass since it is of order of  $s$ . From

$$\hat{s} + \hat{t} + \hat{u} = X^2, \quad (25)$$

one could relate  $x_a$  and  $x_b$ . Using  $X^2 \geq 0$ , maximum and minimum values for  $x_a$  and  $x_b$  are (see Appendix C):

$$x_a^{\min} = \frac{4x_F^2}{4x_F - x_T^2}; \quad x_a^{\max} = 1; \quad (26)$$

$$x_b^{\min} = \frac{k_\perp^2/x}{x_a(1-x)s}; \quad x_b^{\max} = 1, \quad (27)$$

where  $x = x_F/x_a$ .

#### IV. SINGLE-SPIN ASYMMETRY

Consider scattering of the proton with transverse polarization vector  $\vec{a}$  and momentum  $p_+$  and other unpolarized proton with momentum  $p_-$ . In semi-inclusive process the pion with momentum  $k$  is produced.

For the TSSA calculation it is crucial to define a coordinate system, because the sign of TSSA depends on it. We choose the standard right-hand coordinate system. The initial polarized proton moves in  $+z$  direction and its polarization vector is along  $y$  axis, Fig. 2. Positive TSSA means that more pions are produced in  $+x$  half-space when the proton has spin in  $+y$  direction.

Transverse single spin asymmetry (or analyzing power) is defined as

$$A_N = \frac{d\sigma_\uparrow - d\sigma_\downarrow}{d\sigma_\uparrow + d\sigma_\downarrow} = \frac{d\Delta\sigma}{2d\sigma}. \quad (28)$$

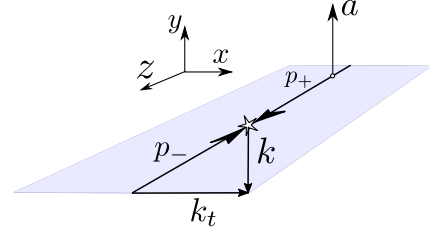


FIG. 2. Kinematics of TSSA. The polarized proton with the momentum  $p_+$  moves in  $+z$ . The polarization vector  $a$  is in  $+y$  or  $-y$  direction. The pion momentum lies in  $zx$  plane.

Arrows  $\uparrow$  and  $\downarrow$  denote the spin polarization vector of the proton in  $+y$  and  $-y$  direction correspondingly. We consider only tree-level diagrams for the unpolarized cross section in the denominator of Eq. (28). As it will be shown later, it is enough to reproduce cross section data. Moreover, we expect that higher orders are suppressed by instanton density and  $\alpha_s$ .

Polarized parton cross section is related with hadron cross section as a convolution with polarized PDFs.

$$d\sigma_\uparrow = \sum_f \iint dx_a dx_b f_{a^\uparrow/A^\uparrow}(x_a) f(x_b) d\hat{\sigma}_\uparrow \quad (29)$$

$$\Delta\sigma = \Delta_T f_{a/A} \otimes f_b \otimes \Delta\hat{\sigma}. \quad (30)$$

$\Delta_T f_{a/A}$  is the transversity distribution—the difference between the probabilities to find parton  $a$  polarized parallel and antiparallel to the polarization of hadron  $A$ .

Transverse polarization state can be represented as superposition of helicity states:

$$|\uparrow\downarrow\rangle = \frac{1}{\sqrt{2}}(|+\rangle \pm i|-\rangle). \quad (31)$$

Using this we can rewrite the difference of amplitudes with opposite transverse polarizations as a product of helicity amplitudes:

$$|\mathcal{M}_\uparrow|^2 - |\mathcal{M}_\downarrow|^2 = 2\text{Im}(\mathcal{M}_+ \mathcal{M}_-^*). \quad (32)$$

$\pm$  mean helicity of initial parton in the polarized proton. We sum over polarization of other particles.  $\mathcal{M}_\pm$  has five parts shown on Fig. 3. Until now both  $\mathcal{M}_+$  and  $\mathcal{M}_-$  contain spin-flip and non-flip amplitudes. But only the interference between spin-flip (a,d,e) and non-flip(b,c) diagrams survives in TSSA. In this light, one could think about  $\mathcal{M}_+ \mathcal{M}_-^*$  as a product of spin-flip and non-flip amplitudes. Leading contribution into  $\Delta\sigma$  comes from interference between (a) and (b+c) diagrams. We expect that the interference between (b+c) and (d+e) diagrams is suppressed due to additional  $\alpha_s$ . Moreover, because they have the same structure, phase shift between them is small.

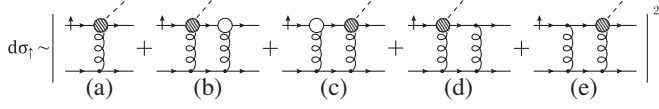


FIG. 3. The set of considered diagrams that give contributions to the total scattering amplitude. Notation for interaction vertices is similar to Fig. 1.

Upper line should have an odd number of chromomagnetic vertices and the bottom line—an even number or all perturbative. First we look at the case with all perturbative vertices on the bottom line.

We use the momentum notation that is shown on Fig. 4. Sudakov's decomposition for momentum vectors is as before, Eq. (7). A new vector  $q_0$  is decomposed as:

$$q_0 = \alpha_0 p_+ + \beta_0 p_- + q_{0\perp}. \quad (33)$$

$\Delta\hat{\sigma}$  is proportional to the interference of spin flip and nonflip diagrams Eq. (32)

$$\Delta\hat{\sigma} = \frac{1}{2\hat{s}} 2 \cdot 2 \sum_{s,c} \text{Im}[\mathcal{A}_+(\mathcal{B}_{1-} + \mathcal{B}_{2-})^*] d\hat{R}_3, \quad (34)$$

Factor  $1/2\hat{s}$  is the flux of initial particles. In the numerator first factor 2 appears because  $\mathcal{A}_+(\mathcal{B}_{1-} + \mathcal{B}_{2-})^* = \mathcal{A}^*(\mathcal{B}_{1+} + \mathcal{B}_{2+})$  [33] and the second from Eq. (32).  $\sum_{s,c}$  symbolically denotes averaging over spin and color states. Three-particles phase space  $d\hat{R}_3$  was calculated before.

Using Gribov decomposition for  $g_{\mu\nu}$  we factorize diagrams to upper and lower parts. The interference between first and second diagram on the Fig. 4 is

$$\begin{aligned} \mathcal{A}_+ \mathcal{B}_{1-}^* &= \frac{1}{2 \cdot 9} \left(\frac{2}{\hat{s}}\right)^3 g_s^3 \frac{C^3}{F_\pi^2} \int \frac{d^4 q_0}{(2\pi)^4} \\ &\times \frac{\text{Tr}[t^a t^b t^c] \text{Tr}[t^{a'} t^{b'} t^{c'}] \delta_{aa'} \delta_{bb'} \delta_{cc'} (U_1 D)}{q^2 q_0^2 (q - q_0)^2 (p_+ + q_0 - k)^2 (p_- - q_0)^2}. \end{aligned} \quad (35)$$

$U_1$  and  $D$  are products of gamma matrices corresponded upper and bottom fermion lines respectively. Factors 2 and 9 in the denominator are from averaging over spins of the unpolarized quark and over color states. The color trace is

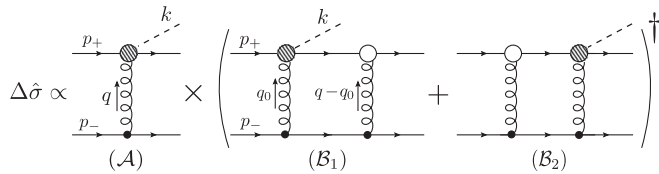


FIG. 4. The leading contribution to TSSA. The left loop diagram we denote as  $\mathcal{B}_1$ , the right one as  $\mathcal{B}_2$ . The tree-level diagram is  $\mathcal{A}$ .

$$\text{Tr}[t^a t^b t^c] \text{Tr}[t^{a'} t^{b'} t^{c'}] \delta_{aa'} \delta_{bb'} \delta_{cc'} = -2/3. \quad (36)$$

We calculate the imaginary part by putting fermions in the loop on mass shell. After collecting all  $i$  and signs in vertices

$$\begin{aligned} \text{Im}(\mathcal{A}\mathcal{B}_1^*) &= -\frac{2/3}{2 \cdot 9} \left(\frac{2}{\hat{s}}\right)^3 g_s^3 \frac{C^3}{F_\pi^2} \int \frac{d^2 q_{0\perp} d\alpha_0 d\beta_0 \hat{s} (-2\pi i)^2}{(2\pi)^4 2 \cdot 2i} \\ &\times \frac{\delta((p_- - q_0)^2) \delta((p_+ + q_0 - k)^2) U_1 D}{q^2 q_0^2 (q_0 - q)^2} \\ &= -\frac{g_s^3 C^3}{54 \hat{s}^4 \pi^2 F_\pi^2} \int \frac{d^2 q_{0\perp}}{(1-x)} \frac{U_1 D}{q_\perp^2 q_{0\perp}^2 (q_{0\perp} - q_\perp)^2}, \end{aligned} \quad (37)$$

where  $d^4 q_0 = \frac{\hat{s}}{2} d\alpha_0 d\beta_0 d^2 q_{0\perp}$  was used. Notice that the loop integral in  $\mathcal{A}\mathcal{B}_1^*$  is restricted by the sphaleron energy, similar to the phase space integral,  $(p_+ + q_0)^2 < E_{\text{sph}}^2$ .

For the upper fermion line we have

$$\begin{aligned} U_1 &= \bar{u}_{p_+}(-) \not{q}_{0\perp} \not{p}_- \gamma_5 (\not{p}_+ + \not{q}_0 - \not{k}) (\not{q}_\perp - \not{q}_{0\perp}) \not{p}_- \\ &\times (\not{p}_+ + \not{q} - \not{k}) \gamma_5 \not{p}_- \not{q}_\perp u_{p_+}(+) \\ &= -2(1-x)^2 \hat{s}^3 (q_{0\perp}^2 q_x - q_\perp^2 q_{0x}), \end{aligned} \quad (38)$$

where subscript  $x$  denotes the component of a vector along  $x$ -axis.  $u(\pm)$  is the spinor for a quark in the corresponded helicity state. For the bottom quark line with all perturbative vertices the trace is

$$D = \text{Tr}[(\not{p}_- - \not{q}) \not{p}_+ \not{p}_- \not{p}_+ (\not{p}_- - \not{q}_0) \not{p}_+] = 2\hat{s}^3. \quad (39)$$

The second contribution shown on Fig. 4 is given by the formula:

$$\text{Im}\mathcal{A}\mathcal{B}_2^* = -\frac{g_s^3 C^3}{54 \hat{s}^4 \pi^2 F_\pi^2} \int d^2 q_{0\perp} \frac{U_2 D}{q_\perp^2 q_{0\perp}^2 (q_{0\perp} - q_\perp)^2}, \quad (40)$$

$$\begin{aligned} U_2 &= \bar{u}_{p_+}(-) \not{q}_{0\perp} \not{p}_- (\not{p}_+ + \not{q}_{0\perp}) (\not{q}_\perp - \not{q}_{0\perp}) \not{p}_- \gamma_5 \\ &\times (\not{p}_+ + \not{q} - \not{k}) \gamma_5 \not{p}_- \not{q}_\perp u_{p_+}(+) \\ &= 2(1-x) \hat{s}^3 (q_{0\perp}^2 q_x - q_\perp^2 q_{0x}). \end{aligned} \quad (41)$$

The absence of additional  $(1-x)$  in the trace  $U_2$  in comparison with  $U_1$  is compensated by lack of  $(1-x)$  in denominator of Eq. (40). The trace  $D$  is the same. Therefore,  $\text{Im}(\mathcal{A}\mathcal{B}_1^*)$  and  $\text{Im}(\mathcal{A}\mathcal{B}_2^*)$  differ by the sign and integration limits over  $d^2 q_{0\perp}$ . Loop integral in  $\mathcal{A}\mathcal{B}_1$  is limited by the sphaleron energy. In contrast, the loop integral in  $\mathcal{A}\mathcal{B}_2$  does not have such limit. Because the integrands are the same in an absolute value and with opposite sign, we can exclude part of the integration region

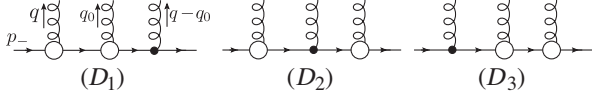


FIG. 5. Additional contributions to TSSA from diagrams with chromomagnetic vertices on the bottom line.

where they are canceled out. Nonzero contribution comes from region where  $(p_+ + q_0)^2 > E_{\text{sph}}^2$ .

Combining these observations, the final result is

$$\frac{d\Delta\hat{\sigma}}{dx d^2k_{\perp}} = \frac{g_s^3}{27 \cdot 2^6 \pi^7} \frac{C^3}{F_{\pi}^2} \int_0^{E_{\text{sph}}^2} dM_k^2 \int_0^{\pi} d\tilde{\phi} \int d^2q_{0\perp} \times \theta(M_0^2 - E_{\text{sph}}^2) \frac{(1-x)}{x^2} \frac{(q_x q_{0\perp}^2 - q_{0x} q_{\perp}^2)}{q_{\perp}^2 q_{0\perp}^2 (q_{0\perp} - q_{\perp})^2}, \quad (42)$$

where  $M_0^2 = (p_+ + q_0)^2$ .

We also calculated contributions to TSSA from diagrams with chromomagnetic vertices on the bottom line (Fig. 5). There are three possible combinations which give for the trace:

$$D_1 = 2s^3(q_{\perp} \cdot q_{0\perp}), \quad (43)$$

$$D_2 = 2s^3(q^2 - (q_{\perp} \cdot q_{0\perp})), \quad (44)$$

$$D_3 = 2s^3(q_0^2 - (q_{\perp} \cdot q_{0\perp})). \quad (45)$$

One should substitute these expressions instead of  $D$  in Eq. (37) and Eq. (40), replacing accordingly couplings  $g_s$  and  $C$ .

## V. NUMERICAL RESULTS AND DISCUSSION

For numerical estimations we use parameters provided by the instanton liquid model for QCD vacuum [28,29]. We choose  $F_{\pi} = 93$  MeV,  $m_q = 90$  MeV,  $\rho_c = 1.6$  GeV $^{-1}$  (0.32 fm). It corresponds to AQCM with the value  $\mu_a = -0.45$  and  $\alpha(\rho_c) \approx 0.6$ . For perturbative coupling we use

$$\alpha_s(q^2) = \frac{4\pi}{9 \ln(q^2/\Lambda_{\text{QCD}}^2)} \theta(q^2 - 1/\rho_c^2), \quad (46)$$

where  $\Lambda_{\text{QCD}} = 200$  MeV. Choice of  $\Lambda_{\text{QCD}}$  does not affect significantly numerical results. The step-function  $\theta$  ‘‘switches off’’ perturbative interaction at momenta lower than the instanton scale. It regularizes the cross section, removing Landau pole, and effectively works as a phenomenological gluon mass. Such procedure can be justified in terms of the potential between quarks. In the Cornell potential the linear term starts to dominate the Coulomb-like term from one gluon exchange at distances more than 0.3 fm.

First, we will discuss results for parton cross section and TSSA in  $qq \rightarrow \pi^0 X$  to demonstrate dynamics not

affected by PDFs. Further we use  $k_t = k_{\perp}$ . Figure 6 shows contributions of different diagrams from Fig. 1 to the  $\pi^0$  production cross section. One could see that at chosen parameters contributions of diagrams (a) and (c) are of the same order while the contribution from (b) is smaller. The slope of the cross section with  $k_t$  is determined by the shape of the form factor  $F_g$ . All three contributions have a similar dependency on  $x$ . As expected, at high  $k_t$  the diagram (a) with the perturbative vertex dominates.

$E_{\text{sph}}$  in Eq. (19) determines minimal  $k_t$  at which the whole quark-pion system has nonzero transverse momentum. When  $|k_t| > E_{\text{sph}}/2$ , the exchanged gluon has to have nonzero transverse momentum  $q_{\perp}$  at any  $x$ . At  $|k_t| \leq E_{\text{sph}}/2$ , momenta  $q_{\perp}$  can be zero and we get divergence. We avoid this by the cut of the perturbative coupling  $\alpha_s$  described above. This determines transition

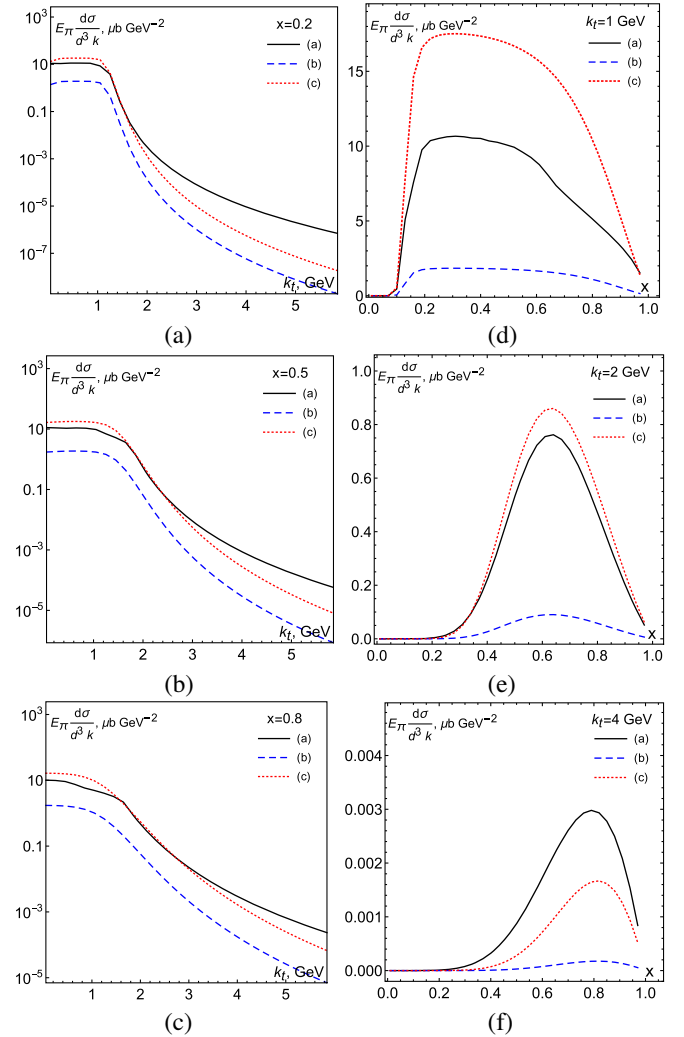


FIG. 6. Differential cross section  $qq \rightarrow \pi^0 X$  as function of  $k_t$  (left column) and  $x$  (right column). Solid line is for the contribution of Fig. 1(a). Dashed line is Fig. 1(b). The dotted line is for the two pion process Fig. 1(c). Parameters are as described in the text.

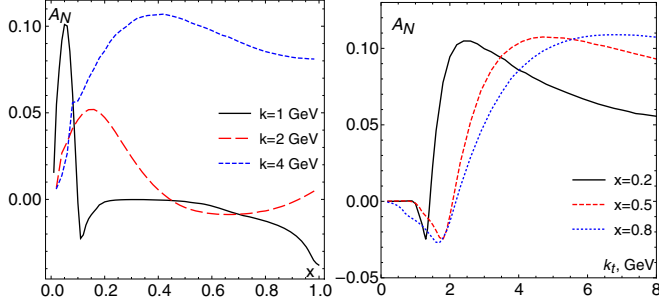


FIG. 7. Pion production asymmetry from scattering of constituent quarks. Left: TSSA as function of  $x$  for different  $x$ . Right: TSSA as function of  $k_\perp$  for  $x = 0.2, 0.5, 0.8$ .

from “flat” behavior of the cross section at small  $k_t < 1.5$  GeV to falling.

Figure 7 shows asymmetry for parton scattering. It is evident that TSSA changes the sign at some  $k_t$ . It is due to the counteracting of two terms in Eq. (42):  $q_x q_0^2$  and  $q_{0x} q^2$ . At small  $k_t$ , the first term dominates.  $q$  grows with  $k_t$ , and the second term overcomes the first one. TSSA reach high value  $\sim 10\%$  at high  $x$  and  $k_t$ . However, for small  $k_t$ ,  $A_N$  has peak at smaller  $x$  and at bigger  $x$  it changes sign.

Figure 8 demonstrates contribution to TSSA from diagrams with chromomagnetic vertices on the bottom line from Fig. 5. These contributions are almost canceled out and the final result does not change significantly.

In order to calculate hadron cross section and asymmetry, we use set of PDFs provided by NNPDF Collaboration [34]. Results on figures are obtained with NLO parton densities (valence+sea quarks) taken at the scale  $Q^2 = 1$  GeV.

Our results for cross section is depicted on Fig. 9 and shows agreement with data at RHIC. Similar pQCD

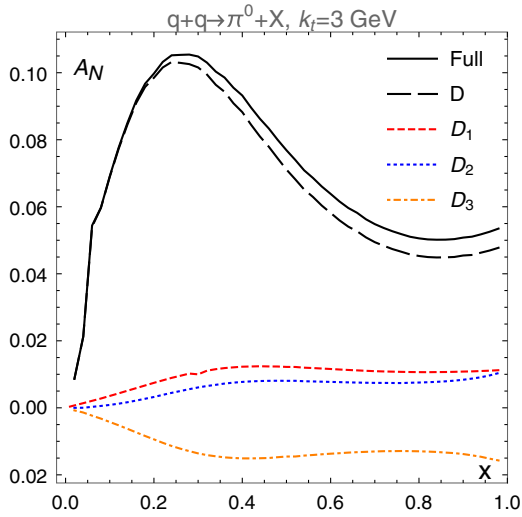


FIG. 8. Contribution of diagrams with AQCM vertex on the bottom line to the parton level TSSA. Solid line is total result, long dashed line is result with perturbative bottom vertices. Lines denoted  $D_i$  correspond to contributions depicted on Fig. 5.

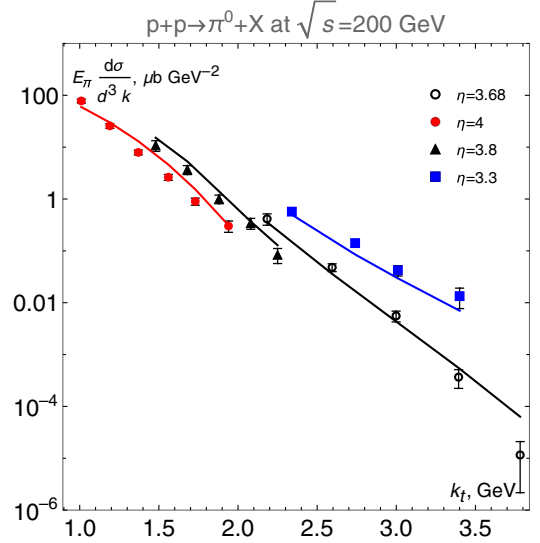


FIG. 9. Differential cross section for  $\pi^0$  production vs  $k_t$  for RHIC. Data are from [5,35].

calculations usually are sensitive to a choice of fragmentation functions and scale. Good agreement of forward rapidity data and NLO pQCD calculation was reported in [35]. However, there DSS fragmentation function [36] has been used, which includes previous RHIC data for fitting. Results of calculation with other fragmentation function, which do not include RHIC forward rapidity data to analysis, usually underestimate the cross section by factor 2 [36]. Overall, for RHIC forward kinematics our model gives predictions similar to pQCD but using less parameters.

Now let us look at TSSA. In a nonrelativistic framework transverse and longitudinal polarized distributions are equal,  $\Delta_T f = \Delta_L f$ , since rotations in spin space between different basis commute with spatial operations. However, relativistically  $\Delta_T f$  and  $\Delta_L f$  are different. Therefore any difference between helicity and transversity PDFs is related to the relativistic nature of parton dynamics inside hadrons. Unfortunately, polarized transverse distribution is poorly known [37]. Instead we use the helicity parton densities  $\Delta_L f$  from NNPDF as an estimation. There are evidences that longitudinal and transverse distributions are the same order [38–40]. Moreover, nucleon’s tensor charge has strong scale dependency and as a result the transversity distribution may inherit this strong evolution [38,41]. In our estimations we do not consider evolution for transversity and unpolarized pdf.

Figure 10 shows results for  $A_N$  at RHIC energies for the neutral pion. Our model predictions are close to data at  $\eta = 3.3$  and slightly underestimate it. At higher rapidity discrepancy becomes bigger.  $A_N$  rises with  $x_F$  with maximum asymmetry  $\approx 10\%$  at  $x_F = 0.8$ . Despite the fact that the model gives the correct trend of growing asymmetry, theoretical curves are shifted in  $k_t$  in comparison with experimental points. One sees a dependency on



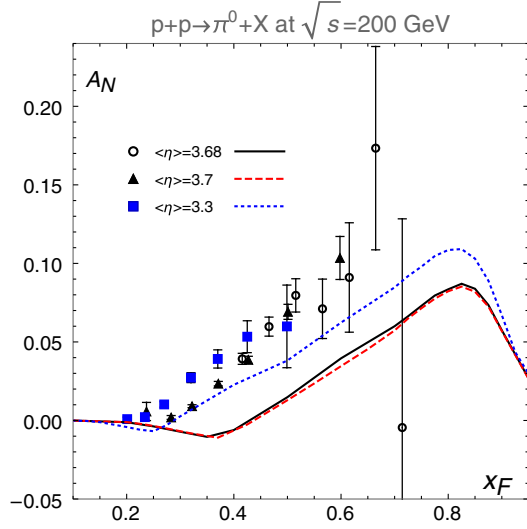


FIG. 10. TSSA for  $\pi^0$  production on RHIC, data are from [35,42].

pseudorapidity, however data do not have such effect. The reason for such behavior in our model is that for the same  $x_F$ ,  $k_t$  decreases with  $\eta$ . It is evident from Fig. 7 that if  $k_t$  is 1–2 GeV asymmetry becomes small or changes the sign. This is what happens at  $\eta = 3.7$  when  $x_F \approx 0.4$  on Fig. 10. In the case  $\eta = 3.3$  it occurs at lower  $x_F$  and is not so noticeable.

Figure 11 shows predictions of our model at different  $x_F$ . Results from the fit of the Sivers function [43] and twist-3 fit from [44] are also shown. Notice that our model, in contrast with others, demonstrates asymmetry growing with  $k_t$ . Similar to Fig. 10, our theoretical curves are shifted to higher  $k_t$  in respect with data points. A possible reason for “shifted” results is an interference with other

diagrams that we neglected in calculation. This effect requires further study.

An additional contribution to TSSA induced by instantons was suggested in the papers [45] and [46,47]. It is based on the results from [48], where the effects of instantons in the nonpolarized DIS process were calculated. In this mechanism the effect arises from phase shift in the quark propagator in the instanton field. This contribution might be complementary to the effect calculated here. Interplay between them could be the reason for overall shift of TSSA to the region of higher  $k_t$ .

Results for the cross section are sensitive to the value of constituent quark mass  $m_q$ , because the nonperturbative coupling is proportional to  $m_q$ . In order to describe cross section data we take  $m_q = 90$  MeV. It is in agreement with the single instanton approximation where  $m_q = 86$  MeV [49]. However, constituent quark masses from the Diakonov-Petrov model ( $m_q = 350$  MeV) [28] and mean field approximation ( $m_q = 170$  MeV) [29] are too big.

The question how does the proposed mechanism interplay with the factorization approach requires additional study. In our model fragmentation and hard rescattering are coherent. It is clear that instanton generated vertices are suppressed at high enough  $k_t$ , factorization restores and fragmentation must appear from some other process, not coherent with hard rescattering. If we assume that this incoherent process is completely contained in fitted fragmentation functions, it is impossible to study the intermediate kinematic region where both of them are at work. We need a model for fragmentation. A possible answer is to calculate fragmentation functions in framework of our model in a way, similar to NJL models [50,51]. If the model gives reasonable results for fragmentation function, it will be possible to study the interplay between coherent and incoherent regimes.

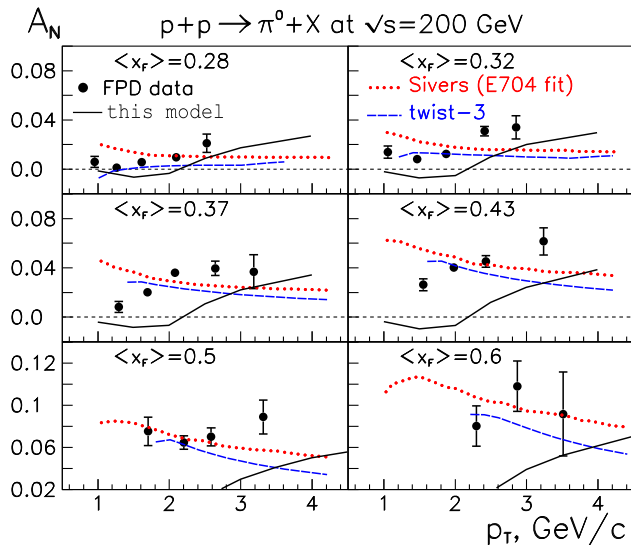


FIG. 11. TSSA at individual  $x_F$  bins. Data are from [42].

## VI. CONCLUSION

We calculated TSSA and cross section for pion production in  $pp$  scattering at RHIC energies using the instanton induced effective interaction. The proposed framework requires less parameters in comparison with the traditional pQCD approach where one needs to parametrize and fit the pion fragmentation function.

Predictions of the model for cross section are consistent with experimental data. Our model produces the big asymmetry at RHIC kinematics, the same magnitude as in experiment. However it is shifted to the region of higher  $k_t$  in respect to data. Remarkable outcome of our approach is increase of the asymmetry with transverse momenta of a final particle at given kinematics. This growth is replaced by a slow decrease at  $k_t > 5$  GeV. Such behavior comes from a rather soft powerlike form factor of effective vertices and a small average size of instanton,  $\rho_c \approx 1/3$  fm, in QCD vacuum. Similar dependence of asymmetry on  $k_t$  is seen in

experiment and was not expected in the models based on TMD factorization and *ad hoc* parametrization of Sivvers and Collins functions.

Another feature of the approach is that  $A_N$  does not depend on c.m. energy. The energy independence of TSSA is observed experimentally and in contradiction with naive expectation that spin effects in strong interaction should vanish at high energy. Moreover, the sign of the TSSA is defined by the sign of AQCM.

Proposed mechanism breaks factorization and can not be treated as an additional contribution to the Sivvers distribution function or to the Collins fragmentation function. In framework of this model, asymmetry in SIDIS and  $pp$  is generated by distinct diagrams and in general could be different. If this effect has place, Sivvers and Collins functions are not universal at small transversal momenta. This phenomenon requires further study.

### ACKNOWLEDGMENTS

The study was supported by the National Natural Science Foundation of China, Grants No. 11975320 (P. M. Z.) and No. 11875296 (N. Korchagin). N. K. thanks the Chinese Academy of Sciences Presidents International Fellowship Initiative for the support via Grants No. 2020PM0073.

### APPENDIX A: PHASE SPACE

In this appendix we give details of phase space calculation for 3- and 4-particle final state. Although it is a standard calculation that can be found in textbooks, in our model phase space is limited.

The phase space for three massless particles with momenta  $q_+$ ,  $q_-$  and  $k$  is

$$\begin{aligned} d\hat{R}_3 &= \frac{(2\pi)^4 \delta^4(p_+ + p_- - k - q_- - q_+)}{(2\pi)^9} \frac{d^3k d^3q_+ d^3q_-}{2E_{q_+} 2E_{q_-} 2E_k} \\ &= \frac{1}{(2\pi)^5} \delta(q_-^2) \frac{d^3k d^3q_+}{2E_k 2E_{q_+}} \\ &= \frac{1}{(2\pi)^5} \delta(k^2) \delta(q_+^2) \delta(q_-^2) d^4k d^4q_+, \end{aligned} \quad (\text{A1})$$

where we used  $d^3p/2E = d^4p\delta(p^2)$  and delta function to remove integration over  $d^4q_-$ .  $E_i$  is the energy of a corresponding particle.

We use the decomposition of momenta vectors on light cone vectors  $p_+$  and  $p_-$ , Eq. (7). From the decomposition and energy-momentum conservation we get the following relations:

$$\begin{aligned} k^2 &= x\beta_k\hat{s} - k_\perp^2; \\ (p_- - q)^2 &= \alpha(\beta - 1)\hat{s} - q_\perp^2; \\ (p_+ + q - k)^2 &= (1 + \alpha - x)(\beta - \beta_k)\hat{s} - (q_\perp - k_\perp)^2; \\ \alpha_+ &= 1 + \alpha - x \approx 1 - x; \\ \beta_- &= 1 - \beta \approx 1; \quad \alpha = -\alpha_-; \\ \beta &= \beta_k + \beta_+. \end{aligned} \quad (\text{A2})$$

$\perp$  denotes 2-dimensional Euclidean vectors which are transverse to the beam axis  $z$ . Using this decomposition, we rewrite  $d\hat{R}_3$  as

$$d\hat{R}_3 = \frac{\hat{s}^2}{4(2\pi)^5 |x\alpha_+(\beta - 1)\hat{s}^3|} \approx \frac{1}{4(2\pi)^5} \frac{dx d^2k_\perp d^2q_\perp}{x(1-x)\hat{s}}, \quad (\text{A3})$$

where  $d\beta \approx d\beta_+$  has been used.

The next step is to change the integration variable  $d^2q_\perp \rightarrow dM_k^2 d\phi$ .  $M_k$  is the invariant mass of the pion  $k$  and  $q_+$  quark:

$$M_k^2 = (p_+ + q)^2 = (1 + \alpha)\beta\hat{s} - q_\perp^2. \quad (\text{A4})$$

Using

$$\alpha \ll 1; \quad \beta = \beta_+ + \beta_k = \frac{q_{+\perp}^2}{(1-x+\alpha)\hat{s}} + \frac{k_\perp^2}{x\hat{s}} \quad (\text{A5})$$

we get that

$$M_k^2 = \frac{(q_\perp - k_\perp)^2}{(1-x)} + \frac{k_\perp^2}{x} - q_\perp^2 = \frac{(xq_\perp - k_\perp)^2}{x(1-x)}. \quad (\text{A6})$$

If we define a new perpendicular vector  $\tilde{q}_\perp$  as

$$\tilde{q}_\perp^2 = (xq_\perp - k_\perp)^2, \quad (\text{A7})$$

we easily can change the integration variable:

$$d^2q_\perp = \frac{d^2\tilde{q}_\perp}{x^2} = \frac{(1-x)}{x} \int_0^{E_{\text{sph}}^2} dM_k^2 \int_0^\pi d\tilde{\phi}. \quad (\text{A8})$$

$E_{\text{sph}} = \frac{3\pi}{2\rho_c}$  is the sphaleron energy which determines the height of potential barriers between different vacuums. The sphaleron energy restricts allowed phase space. The final result for the 3-particle phase space is

$$d\hat{R}_3 = \frac{1}{2^7 \pi^5} \frac{dx d^2k_\perp}{x^2 \hat{s}} \int_0^{E_{\text{sph}}^2} dM_k^2 \int_0^\pi d\tilde{\phi}. \quad (\text{A9})$$

Next, we need the 4-particle phase space for diagram Fig. 1(c). It is given by

$$d\hat{R}_4 = \frac{(2\pi)^4}{(2\pi)^{12}} \times \frac{\delta^4(p_+ + p_- - l - k - q_- - q_+) d^3 k d^3 l d^3 q_+ d^3 q_-}{2E_{q_+} 2E_{q_-} 2E_k 2E_l}. \quad (\text{A10})$$

Using the following relations

$$\begin{aligned} l^2 &= z\alpha_l \hat{s} - l_\perp^2; & k^2 &= x\beta_k \hat{s} - k_\perp^2; \\ \alpha_+ &= 1 + \alpha - x \approx 1 - x; & \beta_- &= 1 - \beta - z \approx 1 - z; \\ \alpha &= -\alpha_- - \alpha_l; & \beta &= \beta_k + \beta_+; \\ \beta_+ &= \frac{q_{+\perp}^2}{\alpha_+ \hat{s}}; & q_{+\perp} &= q_\perp - k_\perp; & \beta_k &= \frac{k_\perp^2}{x \hat{s}}, \end{aligned} \quad (\text{A11})$$

we rewrite the expression for the phase space as

$$\begin{aligned} d\hat{R}_4 &= \frac{\hat{s}^3}{2^3 (2\pi)^8} \frac{dx d^2 k_\perp dz d^2 l_\perp d^2 q_\perp}{\hat{s}^4 |\alpha_+ \beta_- z x|} \\ &\approx \frac{dx dz d^2 k_\perp d^2 l_\perp d^2 q_\perp}{8 (2\pi)^8 \hat{s} x (1-x) z (1-z)}. \end{aligned} \quad (\text{A12})$$

Now we are going to change the integration variable  $d^2 l_\perp \rightarrow dM_l^2 d\phi$ , where  $M_l$  is the invariant mass of the  $l$  pion and  $q_-$  quark system. Notice that here we replace  $d^2 l_\perp$ , not  $d^2 q_\perp$ .

$$\begin{aligned} M_l^2 &= (p_- - q)^2 = -\alpha(1-\beta)\hat{s} - q_\perp^2 \approx (\alpha_- + \alpha_l)\hat{s} - q_\perp^2 \\ &= \frac{(zq_{-\perp} - (1-z)l_\perp)^2}{z(1-z)} - q_\perp^2 = \frac{(zq_\perp + l_\perp)^2}{z(1-z)}, \end{aligned} \quad (\text{A13})$$

where we used  $\alpha_- = \frac{q_{-\perp}^2}{\beta_- \hat{s}} \approx \frac{(q_\perp + l_\perp)^2}{(1-z)\hat{s}}$  and  $\alpha_l = \frac{l_\perp^2}{z\hat{s}}$ . If we define a new momentum  $n_\perp = zq_\perp + l_\perp$ , then we can change integration variable:

$$\int d^2 l_\perp = \int d^2 n_\perp = \int_0^{2\pi} d\phi_n \int \frac{dn_\perp^2}{2} = z(1-z)\pi \int_0^{E_{\text{Sph}}^2} dM_l^2, \quad (\text{A14})$$

where integration over the angle has been performed, because the amplitude does not depend on it. The final result is

$$d\hat{R}_4 = \frac{dx dz d^2 k_\perp d^2 q_\perp dM_l^2}{2^{11} \pi^7 \hat{s} x (1-x)}. \quad (\text{A15})$$

Later, in analogy with  $d\hat{R}_3$  case, we can replace  $d^2 q_\perp \rightarrow dM_k^2 d\tilde{\phi}$ .

## APPENDIX B: AMPLITUDES AND PARTON CROSS SECTIONS

In this appendix we give the details of amplitudes and cross section calculation. The expression for the amplitude shown on Fig. 1(a) is

$$\begin{aligned} |\mathcal{M}_{(a)}|^2 &= \sum_f \sum_{s,c} \overline{g_s} \frac{C(q^2)}{F_\pi} (\bar{u}_{q_+} t^a \sigma_{\mu\nu} q_\nu \gamma_5 u_{p_+}) \\ &\quad \times (\bar{u}_{q_-} i\gamma_\nu t^{a'} u_{p_-}) D_{\mu\nu}^{aa'}(q) \times [\text{H.c.}], \end{aligned} \quad (\text{B1})$$

$$C(q^2) = g_s \frac{\mu_a}{2m_q} F_g(q^2) = -\frac{3\pi^{3/2} \rho_c^2 m_q}{4\sqrt{\alpha_s(\rho_c)}} F_g(q^2), \quad (\text{B2})$$

$$D_{\mu\nu}^{aa'} = -i \frac{g_{\mu\nu} \delta^{aa'}}{q^2}. \quad (\text{B3})$$

Note that  $\alpha_s$  in  $C(q^2)$  is taken at the instanton size scale.  $g_s$  in perturbative vertex is taken at scale  $q^2$ . We omit writing  $q^2$  dependency further.

For a forward scattering, for simplicity of calculation, we use Gribov's decomposition for  $g_{\mu\nu}$ :

$$g_{\mu\nu} = \frac{2p_{+\mu} p_{-\nu}}{\hat{s}} + \frac{2p_{+\nu} p_{-\mu}}{\hat{s}} + g_\perp^{\mu\nu} \approx \frac{2p_{+\mu} p_{-\nu}}{\hat{s}}. \quad (\text{B4})$$

It allows us to make the following replacement:

$$D_{\mu\nu}^{aa'} = -i \frac{2p_{+\mu} p_{-\nu} \delta^{aa'}}{\hat{s} q^2}. \quad (\text{B5})$$

That replacement isolates the leading contributions to the amplitude in power of  $\hat{s}$ . It leads to the substitution in trace formulas:

$$\begin{aligned} \gamma_\mu &\rightarrow \not{p}_-; & \sigma_{\mu\nu} q_\nu &\rightarrow \not{p}_- \not{q}_\perp \text{ for the upper fermionic line,} \\ \gamma_\mu &\rightarrow \not{p}_+; & \sigma_{\mu\nu} q_\nu &\rightarrow \not{p}_+ \not{q}_\perp \text{ for the bottom line,} \end{aligned} \quad (\text{B6})$$

which factorize traces over fermion lines. Using it we get

$$\begin{aligned} |\mathcal{M}_{(a)}|^2 &= \sum_f \frac{1}{4} \frac{\text{Tr}[t^a t^b] \text{Tr}[t^{a'} t^{b'}] \delta^{aa'} \delta^{bb'}}{9} g_s^2 \frac{C^2}{F_\pi^2} \frac{4}{\hat{s}^2} \frac{1}{q^4} \\ &\quad \times \text{Tr}[q_+(p_- \not{q} \gamma_5) \not{p}_+ (-\gamma_5 \not{q} \not{p}_-)] \text{Tr}[q_- \not{p}_+ \not{p}_- \not{p}_+] \\ &= \sum_f \frac{2}{4 \cdot 9} g_s^2 \frac{C^2}{F_\pi^2} \frac{16\hat{s}^2 (1-x) q_\perp^2}{q_\perp^4}, \end{aligned} \quad (\text{B7})$$

where the traces are

$$\begin{aligned} &\text{Tr}[q_+(p_- \not{q}_\perp \gamma_5) \not{p}_+ (-\gamma_5 \not{q}_\perp \not{p}_-)] \\ &= q_\perp^2 \text{Tr}[q_+ \not{p}_- \not{p}_+ \not{p}_-] \\ &= 2q_\perp^2 (1-x+\alpha)\hat{s}^2 \approx 2q_\perp^2 (1-x)\hat{s}^2, \end{aligned} \quad (\text{B8})$$

$$\text{Tr}[\not{q}_-\not{p}_+\not{p}_-\not{p}_+] = 4 \cdot 2q_-p_+ \frac{\hat{s}}{2} = 2(1-\beta)\hat{s}^2 \approx 2\hat{s}^2. \quad (\text{B9})$$

We keep the sum over flavor to indicate, that expressions for  $\pi^\pm$ ,  $\pi^0$  are different.

In the case with the nonperturbative vertex at the bottom line Fig. 1(b), the corresponding trace is

$$\begin{aligned} \text{Tr}[\not{q}_-\not{p}_+\not{q}_\perp\not{p}_-\not{q}_\perp\not{p}_+] &= q_\perp^2 \text{Tr}[\not{q}_-\not{p}_+\not{p}_-\not{p}_+] \\ &= 2(1-\beta)\hat{s}^2 q_\perp^2 \approx 2q_\perp^2 \hat{s}^2. \end{aligned} \quad (\text{B10})$$

$$\begin{aligned} |\mathcal{M}_{(c)}|^2 &= \sum_f \sum_{s,c} -\frac{C^2}{F_\pi^2} (\bar{u}_{q_+} \sigma_{\mu\lambda} q_\lambda \gamma_5 t^a u_{p_+}) (\bar{u}_{q_-} \sigma_{\nu\rho} q_\rho \gamma_5 t^a u_{p_-}) D_{\mu\nu}^{aa'}(q^2) \times [\text{H.c.}] \\ &= \sum_f \frac{C^4}{F_\pi^4} \frac{\text{Tr}[t^a t^b] \text{Tr}[t^{a'} t^{b'}]}{4 \times 9} \delta^{aa'} \delta^{bb'} \frac{4}{\hat{s}^2} \text{Tr}[\not{q}_+(\not{p}_-\not{q}_\perp\gamma_5)\not{p}_+(-\gamma_5\not{q}_\perp\not{p}_-)] \text{Tr}[\not{q}_-(\not{p}_+\not{q}_\perp\gamma_5)\not{p}_-(-\gamma_5\not{q}_\perp\not{p}_+)] \\ &= \sum_f \frac{8\hat{s}^2 C^4}{9F_\pi^4} q_\perp^4 \frac{(1-x)(1-z)}{q_\perp^4}. \end{aligned} \quad (\text{B12})$$

Final formulas for the parton cross section are

$$d\hat{\sigma}_{(a)} = \sum_f \int_0^{E_{\text{sph}}^2} dM_k^2 \int_0^\pi d\tilde{\phi} \frac{g_s^2 C^2}{9(2\pi)^5 F_\pi^2 q_\perp^2 x^2} dx d^2 k_\perp, \quad (\text{B13})$$

$$d\hat{\sigma}_{(b)} = \sum_f \int_0^{E_{\text{sph}}^2} dM_k^2 \int_0^\pi d\tilde{\phi} \frac{C^4}{9(2\pi)^5 F_\pi^2 x^2} dx d^2 k_\perp. \quad (\text{B14})$$

with perturbative and chromomagnetic bottom vertices respectively.

In case of two pions we have

$$\begin{aligned} d\hat{\sigma}_{(c)} &= \frac{|\mathcal{M}_{(c)}|^2}{2\hat{s}} d\hat{R}_4 \\ &= \sum_f \int \frac{C^4}{9F_\pi^4} \frac{(1-z)}{2^9 \pi^7 x} dM_l^2 dx dz d^2 k_\perp d^2 q_\perp \end{aligned} \quad (\text{B15})$$

$$= \sum_f \frac{C^4}{9F_\pi^4} \frac{(1-z)}{2^9 \pi^7 x} E_{\text{sph}}^2 dx dz d^2 k_\perp d^2 q_\perp, \quad (\text{B16})$$

where integration over  $dM_l^2$  was done and we got  $E_{\text{sph}}^2$  in the last line. Next we will integrate out  $dz$ , which gives the factor  $1/2$ :

$$d\hat{\sigma}_{(c)} = \sum_f \frac{C^4}{9F_\pi^4} \frac{E_{\text{sph}}^2 dx d^2 k_\perp d^2 q_\perp}{2^{10} \pi^7 x}. \quad (\text{B17})$$

Repeating similar calculations we get

$$|\mathcal{M}_{(b)}|^2 = \sum_f \frac{2}{4 \cdot 9} \frac{C^4 16\hat{s}^2 (1-x) q_\perp^4}{F_\pi^2 q_\perp^4}. \quad (\text{B11})$$

The amplitude for the two pion contribution  $2q \rightarrow 2\pi 2q$  Fig. 1(c) is very similar to the case with one pion vertex. The difference is only in the trace over the bottom fermion line, which becomes similar to the upper line.

Replacing integration over  $d^2 q_\perp$  by  $dM_k^2$  we get:

$$d\hat{\sigma}_{(c)} = \sum_f \frac{C^4 E_{\text{sph}}^2}{9 \times 2^{10} \pi^7 F_\pi^4} \frac{(1-x)}{x^2} dx d^2 k_\perp dM_k^2 d\tilde{\phi}. \quad (\text{B18})$$

In the end let us briefly discuss flavor summation. Pion field in flavor space decomposed as

$$\vec{\tau} \vec{\phi} = \sqrt{2}(\tau_+ \pi^+ + \tau_- \pi^-) + \tau_0 \pi^0, \quad (\text{B19})$$

$$\tau^+ = \begin{pmatrix} 0 & 1 \\ 0 & 0 \end{pmatrix}, \quad \tau^- = \begin{pmatrix} 0 & 0 \\ 1 & 0 \end{pmatrix}, \quad \tau^0 = \begin{pmatrix} 1 & 0 \\ 0 & -1 \end{pmatrix}. \quad (\text{B20})$$

For  $\pi^0$

$$\begin{aligned} |M_{\pi^0}|^2 &\propto (\bar{\psi}_u(\dots)\psi_u - \bar{\psi}_d(\dots)\psi_d)(\bar{\psi}_u(\dots)\psi_u - \bar{\psi}_d(\dots)\psi_d)^* \\ &= (\bar{\psi}_u(\dots)\psi_u)^2 + (\bar{\psi}_d(\dots)\psi_d)^2, \end{aligned} \quad (\text{B21})$$

where (...) denotes any expression with Dirac  $\gamma$  matrices. For charged pions it is

$$\begin{aligned} |M_{\pi^\pm}|^2 &\propto \sqrt{2}(\bar{\psi}_{u,d}(\dots)\psi_{d,u})\sqrt{2}(\bar{\psi}_{u,d}(\dots)\psi_{d,u})^* \\ &= 2(\bar{\psi}_{u,d}(\dots)\psi_{d,u})^2. \end{aligned} \quad (\text{B22})$$

### APPENDIX C: INTEGRATION OVER PARTON MOMENTA FRACTION

A differential hadron cross section is a convolution of parton distribution functions (PDF) and the partonic cross section  $d\hat{\sigma}$

$$d\sigma = \int dx_a dx_b f(x_a) f(x_b) d\hat{\sigma}. \quad (\text{C1})$$

The momenta of an exclusive hadron in the parton c.m. frame and hadron c.m. frame are related:

$$\begin{aligned} \hat{k}_z &= x \frac{\sqrt{\hat{s}}}{2}; & k_z &= x_F \frac{\sqrt{s}}{2} \\ E_k &= \sqrt{k_\perp^2 + k_z^2 + m_\pi^2} \approx \frac{\sqrt{s}}{2} \sqrt{x_T^2 + x_F^2}; \\ x_{T,F} &= \frac{2}{\sqrt{s}} k_{\perp,z}; & x_F &= x_a x; \\ k_z &= \sqrt{\frac{x_a}{x_b}} \hat{k}_z; & k_\perp &= \hat{k}_\perp. \end{aligned} \quad (\text{C2})$$

The hat denotes a value in the parton c.m. frame. Rewriting the cross section in terms of momenta in the hadron frame we get

$$E_k \frac{d^3\sigma}{d^3k} = \sum_f \int_{x_a^{\min}}^{x_a^{\max}} dx_a \int_{x_b^{\min}}^{x_b^{\max}} dx_b f(x_a) f(x_b) \frac{2E_k}{\sqrt{s} x_a} \frac{d\hat{\sigma}}{dx d^2k_\perp}. \quad (\text{C3})$$

We have  $2 \rightarrow 3$  or  $2 \rightarrow 4$  parton subprocess. It means that we cannot recklessly use  $\hat{s} + \hat{t} + \hat{u} = 0$ , which is true for  $2 \rightarrow 2$  subprocess with massless particles. However, we can combine all particles, except the detected one, into an effective particle and reduce our case to  $2 \rightarrow 2$ . We denote the mass of the effective particle as  $X^2$ .

$$\hat{s} + \hat{t} + \hat{u} = X^2, \quad (\text{C4})$$

$$X^2 = (p_+ + p_- - k)^2 = (1-x)\hat{s} - \frac{k_\perp^2}{x}. \quad (\text{C5})$$

For the cross section with one pion we combine only  $q_-$  and  $q_+$  quarks. All formulas are valid for this case also, because we can just put  $l = 0$ . Note that  $\hat{t}$  is not a gluon virtuality,  $\hat{t} \neq q^2$ .

We need express parton variables through hadron level variables:

$$\hat{s} = x_a x_b s; \quad \hat{t} = x_a t; \quad \hat{u} = x_b u; \quad (\text{C6})$$

$$x_1 = -\frac{u}{s} = \frac{x_T}{2 \tan(\theta_h/2)}; \quad (\text{C7})$$

$$x_2 = -\frac{t}{s} = \frac{x_T \tan(\theta_h/2)}{2}. \quad (\text{C8})$$

$\theta_h$  is the pion scattering angle in the hadron c.m. frame.

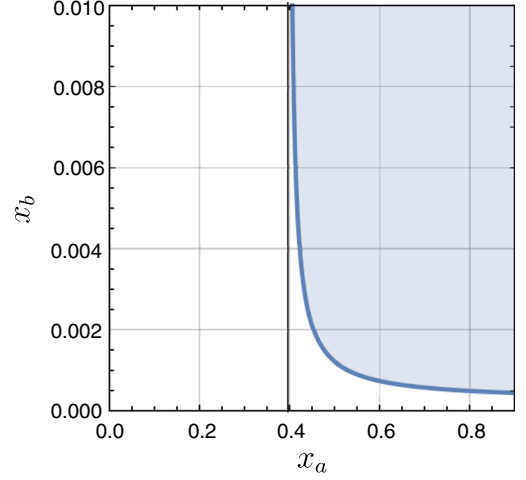


FIG. 12. Integration region over  $x_a$  and  $x_b$  (shaded area) for kinematics  $\sqrt{s} = 200$  GeV,  $k_\perp = 2$  GeV,  $\eta = 3.68$ .

To determine maximum and minimum values for  $x_a$  and  $x_b$ , we notice from Eq. (C4)

$$x_b = \frac{X^2/s + x_a x_2}{x_a - x_1}. \quad (\text{C9})$$

For fixed  $X$ , it is monotonically decreasing function with  $x_a$ . Therefore  $x_a = x_a^{\min}$  when  $x_b = 1$ ,

$$\begin{aligned} x_a^{\min} &= \frac{x_1}{1 - x_2}; & x_a^{\max} &= 1; \\ x_b^{\min} &= \frac{x_a x_2}{x_a - x_1}; & x_b^{\max} &= 1. \end{aligned} \quad (\text{C10})$$

This limits allow kinematic region where invariant mass  $X^2$  becomes negative. We need additional constraints coming from  $X^2 > 0$ :

$$x_b > \frac{k_\perp^2/x}{x_a(1-x)s}. \quad (\text{C11})$$

However, it is not important for RHIC kinematics. Integration region is almost identical to one determined by Eq. (C10) alone. The Fig. 12 shows the example of integration region over  $x_a$  and  $x_b$ .

One may notice that for the amplitude with two pions Fig. 1(c)  $X^2 = (q_+ + q_-)^2$ , without inclusion of the pion  $l$ . As result, limits for  $x_{a,b}$  depend on  $l_\perp$  and  $z$ . Therefore we cannot integrate over  $z$  and  $l_\perp$  independently as we did in (B17). That more rigorous calculation was done and the correction is less than 5% for cross section at the RHIC kinematics. Therefore we can use this approach as a good approximation.

- [1] G. Bunce, R. Handler, R. March, P. Martin, L. Pondrom, M. Sheaff, K. J. Heller, O. Overseth, P. Skubic, and T. Devlin *et al.*,  $\Lambda^0$  Hyperon Polarization in Inclusive Production by 300 – GeV Protons on Beryllium, *Phys. Rev. Lett.* **36**, 1113 (1976)
- [2] G. L. Kane, J. Pumplin, and W. Repko, Transverse Quark Polarization in Large- $p_T$  Reactions,  $e^+e^-$  Jets, and Lepton-production: A Test of QCD, *Phys. Rev. Lett.* **41**, 1689 (1978).
- [3] U. D’Alesio and F. Murgia, Azimuthal and single spin asymmetries in hard scattering processes, *Prog. Part. Nucl. Phys.* **61**, 394 (2008).
- [4] D. L. Adams *et al.* (FNAL-E704 Collaboration), Analyzing power in inclusive  $\pi^+$  and  $\pi^-$  production at high  $x_F$  with a 200 GeV polarized proton beam, *Phys. Lett. B* **264**, 462 (1991).
- [5] J. Adams *et al.* (STAR Collaboration), Forward Neutral Pion Production in p + p and d + Au Collisions at  $\sqrt{s_{NN}} = 200$  GeV, *Phys. Rev. Lett.* **97**, 152302 (2006).
- [6] T. C. Rogers and P. J. Mulders, No generalized TMD-factorization in hadro-production of high transverse momentum hadrons, *Phys. Rev. D* **81**, 094006 (2010).
- [7] J. C. Collins, D. E. Soper, and G. F. Sterman, Transverse momentum distribution in Drell-Yan pair and W and Z boson production, *Nucl. Phys.* **B250**, 199 (1985).
- [8] J. C. Collins and D. E. Soper, Back-to-back jets: Fourier transform from B to K-transverse, *Nucl. Phys.* **B197**, 446 (1982).
- [9] J. C. Collins, Leading twist single transverse-spin asymmetries: Drell-Yan and deep inelastic scattering, *Phys. Lett. B* **536**, 43 (2002).
- [10] A. Metz, Gluon-exchange in spin-dependent fragmentation, *Phys. Lett. B* **549**, 139 (2002).
- [11] C. J. Bomhof, P. J. Mulders, and F. Pijlman, Gauge link structure in quark-quark correlators in hard processes, *Phys. Lett. B* **596**, 277 (2004).
- [12] D. Boer, P. J. Mulders, and F. Pijlman, Universality of T odd effects in single spin and azimuthal asymmetries, *Nucl. Phys.* **B667**, 201 (2003).
- [13] A. A. Henneman, D. Boer, and P. J. Mulders, Evolution of transverse momentum dependent distribution and fragmentation functions, *Nucl. Phys.* **B620**, 331 (2002).
- [14] R. Kundu and A. Metz, Higher twist and transverse momentum dependent parton distributions: A light front Hamiltonian approach, *Phys. Rev. D* **65**, 014009 (2001).
- [15] E. Moffat, W. Melnitchouk, T. C. Rogers, and N. Sato, What are the low- $Q$  and large- $x$  boundaries of collinear QCD factorization theorems? *Phys. Rev. D* **95**, 096008 (2017).
- [16] J. C. Collins, Fragmentation of transversely polarized quarks probed in transverse momentum distributions, *Nucl. Phys.* **B396**, 161 (1993).
- [17] M. Anselmino, M. Boglione, U. D’Alesio, E. Leader, S. Melis, F. Murgia, and A. Prokudin, On the role of Collins effect in the single spin asymmetry  $A_N$  in  $p^\uparrow p \rightarrow hX$  processes, *Phys. Rev. D* **86**, 074032 (2012).
- [18] B. Q. Ma, I. Schmidt, and J. J. Yang, Collins effect in single spin asymmetries of the  $p^\uparrow p \rightarrow \pi X$  process, *Eur. Phys. J. C* **40**, 63 (2005).
- [19] D. W. Sivers, Single spin production asymmetries from the hard scattering of point-like constituents, *Phys. Rev. D* **41**, 83 (1990).
- [20] M. Anselmino, M. Boglione, U. D’Alesio, S. Melis, F. Murgia, and A. Prokudin, Sivers effect and the single spin asymmetry  $A_N$  in  $p^\uparrow p \rightarrow hX$  processes, *Phys. Rev. D* **88**, 054023 (2013).
- [21] M. Anselmino, M. Boglione, and F. Murgia, Single spin asymmetry for  $p^\uparrow p \rightarrow \pi X$  in perturbative QCD, *Phys. Lett. B* **362**, 164 (1995).
- [22] A. V. Efremov and O. V. Teryaev, On spin effects in quantum chromodynamics, *Sov. J. Nucl. Phys.* **36**, 140 (1982), <https://inspirehep.net/literature/167526>.
- [23] J. w. Qiu and G. F. Sterman, Single transverse spin asymmetries in hadronic pion production, *Phys. Rev. D* **59**, 014004 (1998).
- [24] Y. Kanazawa and Y. Koike, Chiral odd contribution to single transverse spin asymmetry in hadronic pion production, *Phys. Lett. B* **478**, 121 (2000).
- [25] N. Kochelev and N. Korchagin, Anomalous quark chromomagnetic moment and single-spin asymmetries, *Phys. Lett. B* **729**, 117 (2014).
- [26] N. Kochelev, H. J. Lee, B. Zhang, and P. Zhang, Gluonic structure of the constituent quark, *Phys. Lett. B* **757**, 420 (2016).
- [27] N. I. Kochelev, Anomalous quark chromomagnetic moment induced by instantons, *Phys. Lett. B* **426**, 149 (1998).
- [28] D. Diakonov, Instantons at work, *Prog. Part. Nucl. Phys.* **51**, 173 (2003).
- [29] T. Schäfer and E. V. Shuryak, Instantons in QCD, *Rev. Mod. Phys.* **70**, 323 (1998).
- [30] E. Witten, Baryons in the 1/n expansion, *Nucl. Phys.* **B160**, 57 (1979).
- [31] N. Kochelev, H. J. Lee, B. Zhang, and P. Zhang, Anomalous pion production induced by nontrivial topological structure of QCD vacuum, *Phys. Rev. D* **92**, 034025 (2015).
- [32] I. Zahed, Scattering through QCD sphalerons, *Nucl. Phys.* **A715**, 887 (2003).
- [33] L. J. Dixon, A brief introduction to modern amplitude methods, <https://doi.org/10.5170/CERN-2014-008.31>.
- [34] E. R. Nocera, R. D. Ball, S. Forte, G. Ridolfi, and J. Rojo (NNPDF Collaboration), A first unbiased global determination of polarized PDFs and their uncertainties, *Nucl. Phys.* **B887**, 276 (2014).
- [35] L. Adamczyk *et al.* (STAR Collaboration), Transverse single-spin asymmetry and cross-section for  $\pi^0$  and  $\eta$  mesons at large Feynman- $x$  in polarized  $p + p$  collisions at  $\sqrt{s} = 200$  GeV, *Phys. Rev. D* **86**, 051101 (2012).
- [36] D. de Florian, R. Sassot, and M. Stratmann, Global analysis of fragmentation functions for pions and kaons and their uncertainties, *Phys. Rev. D* **75**, 114010 (2007).
- [37] M. Radici, A. M. Ricci, A. Bacchetta, and A. Mukherjee, Exploring universality of transversity in proton-proton collisions, *Phys. Rev. D* **94**, 034012 (2016).
- [38] V. Barone, A. Drago, and P. G. Ratcliffe, Transverse polarisation of quarks in hadrons, *Phys. Rep.* **359**, 1 (2002).
- [39] M. Gockeler *et al.* (QCDSF and UKQCD Collaborations), Quark helicity flip generalized parton distributions from two-flavor lattice QCD, *Phys. Lett. B* **627**, 113 (2005).
- [40] S. Aoki, M. Doui, T. Hatsuda, and Y. Kuramashi, Tensor charge of the nucleon in lattice QCD, *Phys. Rev. D* **56**, 433 (1997).

- [41] M. Wakamatsu, Chiral-odd GPDs, transversity decomposition of angular momentum, and tensor charges of the nucleon, *Phys. Rev. D* **79**, 014033 (2009).
- [42] B. I. Abelev *et al.* (STAR Collaboration), Forward Neutral Pion Transverse Single Spin Asymmetries in  $p + p$  Collisions at  $\sqrt{s} = 200$  GeV, *Phys. Rev. Lett.* **101**, 222001 (2008).
- [43] M. Anselmino, M. Boglione, U. D'Alesio, A. Kotzinian, F. Murgia, and A. Prokudin, Extracting the Sivers function from polarized SIDIS data and making predictions, *Phys. Rev. D* **72**, 094007 (2005); Erratum, *Phys. Rev. D* **72**, 099903 (2005).
- [44] C. Kouvaris, J. W. Qiu, W. Vogelsang, and F. Yuan, Single transverse-spin asymmetry in high transverse momentum pion production in  $pp$  collisions, *Phys. Rev. D* **74**, 114013 (2006).
- [45] D. Ostrovsky and E. Shuryak, Instanton-induced azimuthal spin asymmetry in deep inelastic scattering, *Phys. Rev. D* **71**, 014037 (2005).
- [46] Y. Qian and I. Zahed, Single spin asymmetry through QCD instantons, *Phys. Rev. D* **86**, 014033 (2012); Erratum, *Phys. Rev. D* **86**, 059902 (2012).
- [47] Y. Qian and I. Zahed, Spin physics through QCD instantons, *Ann. Phys. (Amsterdam)* **374**, 314 (2016).
- [48] S. Moch, A. Ringwald, and F. Schrempp, Instantons in deep inelastic scattering: The simplest process, *Nucl. Phys.* **B507**, 134 (1997).
- [49] P. Faccioli and E. V. Shuryak, Systematic study of the single instanton approximation in QCD, *Phys. Rev. D* **64**, 114020 (2001).
- [50] D. J. Yang and H. n. Li, Gluon fragmentation functions in the Nambu–Jona-Lasinio model, *Phys. Rev. D* **94**, 054041 (2016).
- [51] S. I. Nam and C. W. Kao, Fragmentation and quark distribution functions for the pion and kaon with explicit flavor-SU(3)-symmetry breaking, *Phys. Rev. D* **85**, 094023 (2012).